Science Advances
AAAS

Supplementary Materials for

Corticotropin-releasing hormone neurons control trigeminal neuralgia-induced anxiodepression via a hippocampus-to-prefrontal circuit

Su-Su Lv *et al.*

Corresponding author: Yu-Qiu Zhang, yuqiuzhang@fudan.edu.cn

Sci. Adv. **10**, eadj4196 (2024)
DOI: 10.1126/sciadv.adj4196

The PDF file includes:

Other Supplementary Material for this manuscript includes the following:

Supplementary Figures

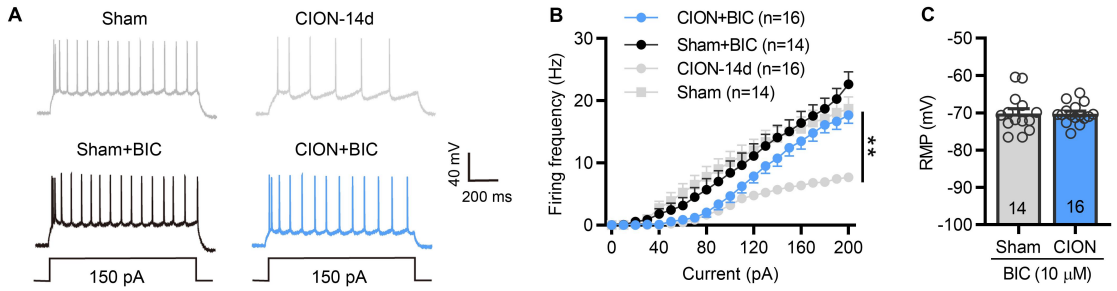

Fig. S1. Blockade of $GABA_A$ receptors reverses the decrease in excitatory of layer V mPFC pyramidal neurons induced by trigeminal neuralgia. (A) Examples of action potentials (APs) traces evoked by depolarizing current in layer V mPFC pyramidal neurons in the presence and absence of $GABA_A$ receptor antagonist bicuculine (BIC, 10 μM) in sham and CION-14d mice. **(B)** Bath application of BIC (10 μM) significantly reversed the decreases firing frequency of APs evoked by depolarizing current steps of mPFC layer V pyramidal neurons in CION-14 mice, but has not effect on the input-output curves of APs in sham mice. $^{**}P<0.01$, two-way RM ANOVA. Here, the gray line data (sham and CION-14d) are from Fig. 1C (sham and CION-14d) as a reference for BIC treatment group. **(C)** The effect of BIC on resting membrane potential (RMP) of layer V mPFC pyramidal neurons of sham- and CION-14d mice. Two-tailed Student's *t*-test. Data are expressed as means ± SEM. Sample sizes are indicated in brackets and bars.

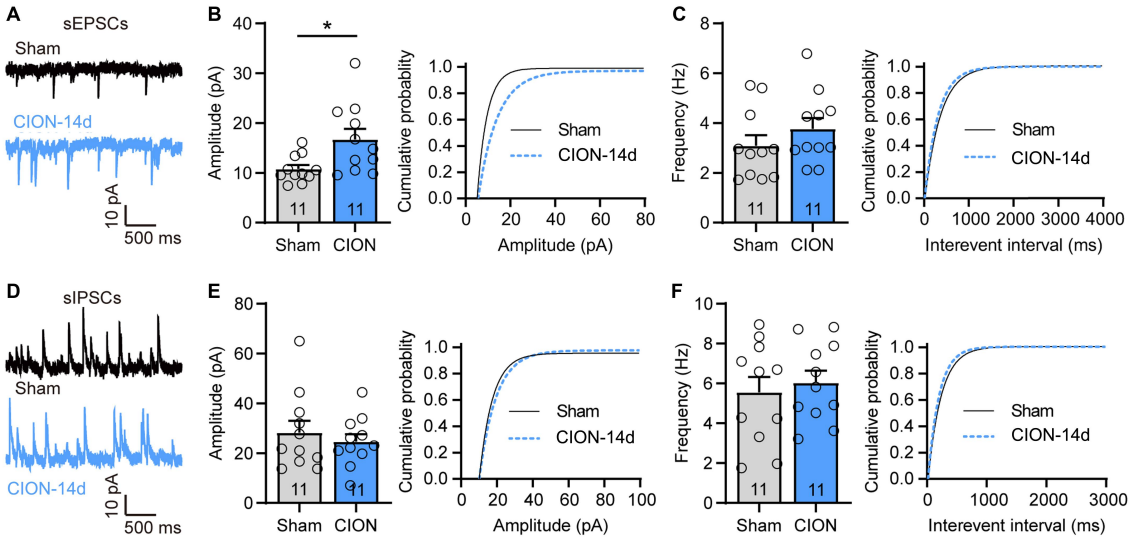

Fig. S2. Trigeminal neuralgia increases excitatory synaptic transmission of vHPC CaMK2A$^+$ neurons. (A-C) Patch clamp recording of spontaneous EPSCs (sEPSCs) showing an increased amplitude of sEPSCs and a right-shifted the cumulative fraction without changes in the frequency and corresponding cumulative fraction in vHPC CaMK2A$^+$ neurons from CION-14d mice. **P*<0.05, two-tailed Student's *t*-test. **(D-F)** Patch clamp recording of spontaneous IPSCs (sIPSCs) showing no difference in amplitude and frequency of sIPSCs in vHPC CaMK2A$^+$ neurons between sham- and CION-14d mice. Two-tailed Student's *t*-test. Data are expressed as means ± SEM. Sample sizes are indicated in bars.

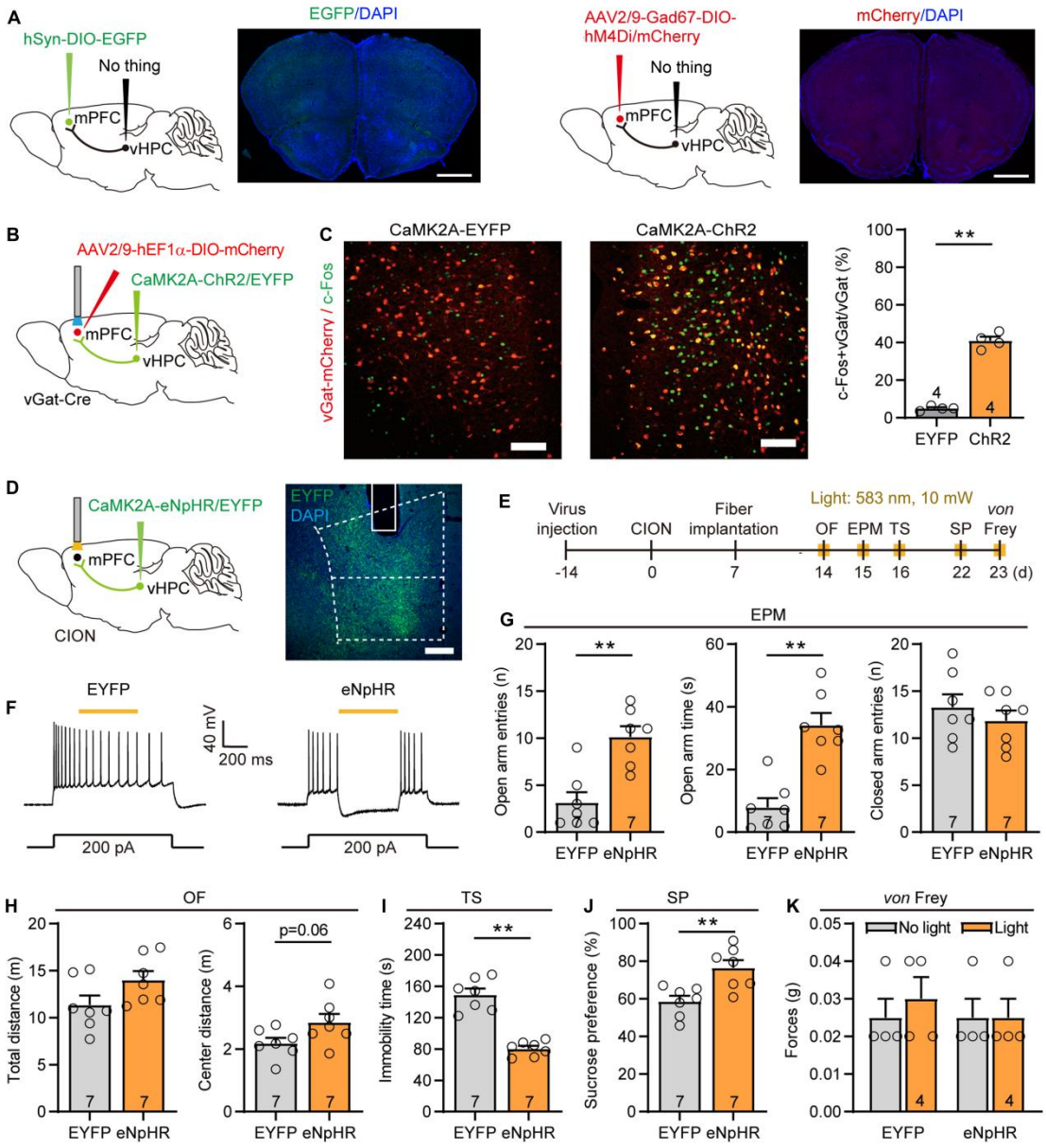

Fig. S3. Optogenetic inhibition of vHPC^{CaMK2A}-mPFC projections improves CION-induced anxiodepressive-like behaviors. (A) Sagittal schematics and photomicrographs showing the specificity of AAV2/1-hSyn-Cre virus. When hSyn-DIO-EGFP (left) or Gad67-DIO-hM4Di-mCherry (right) virus was injected into the mPFC without injecting AAV2/1-hSyn-Cre into the vHPC, no EGFP^{+} (left) or mCherry^{+} (right) neurons were observed in the mPFC. Scale bar: 1 mm. **(B)** Sagittal schematic

showing specific infection of mCherry on mPFC $vGat^{+}$ neurons, and optogenetic manipulation of $vHPC^{CaMK2A}$-positive terminals expressing ChR2 in the mPFC in vGat-Cre mice. **(C)** Optogenetic activation of vHPC CaMK2A -positive terminals expressing ChR2 in the mPFC significantly upregulates c-Fos expression in $vGat^{+}$ neurons in the mPFC. Scale bar: 100 μm. **P<0.01, two-tailed Student's t-test. **(D)** Sagittal schematic and photomicrograph of coronal section showing infection of vHPC CaMK2A -positive terminals in the mPFC with eNpHR or EYFP. Scale bar: 200 μm. **(E)** Schematic of the protocol in experiments G-K. **(F)** Patch clamp recording in vHPC slices showing that APs are suppressed by yellow light stimulation (583 nm, 10 mW, continuous) in vHPC $CaMK2A^{+}$ neurons expressing eNpHR. **(G-J)** Optogenetic inhibition of $vHPC^{CaMK2A}$ -positive terminals in the mPFC ameliorates anxiodepressive-like behaviors in CION mice in elevated plus maze (EPM, G), open field (OF, H), tail suspension (TS, I) and sucrose preference (SP, J) tests. **P<0.01, two-tailed Student's t-test. **(K)** Optogenetic inhibition of $vHPC^{CaMK2A}$-positive terminals in the mPFC does not affect CION-induced mechanical allodynia. Two-way ANOVA. Data are expressed as means ± SEM. Sample sizes are indicated in bars.

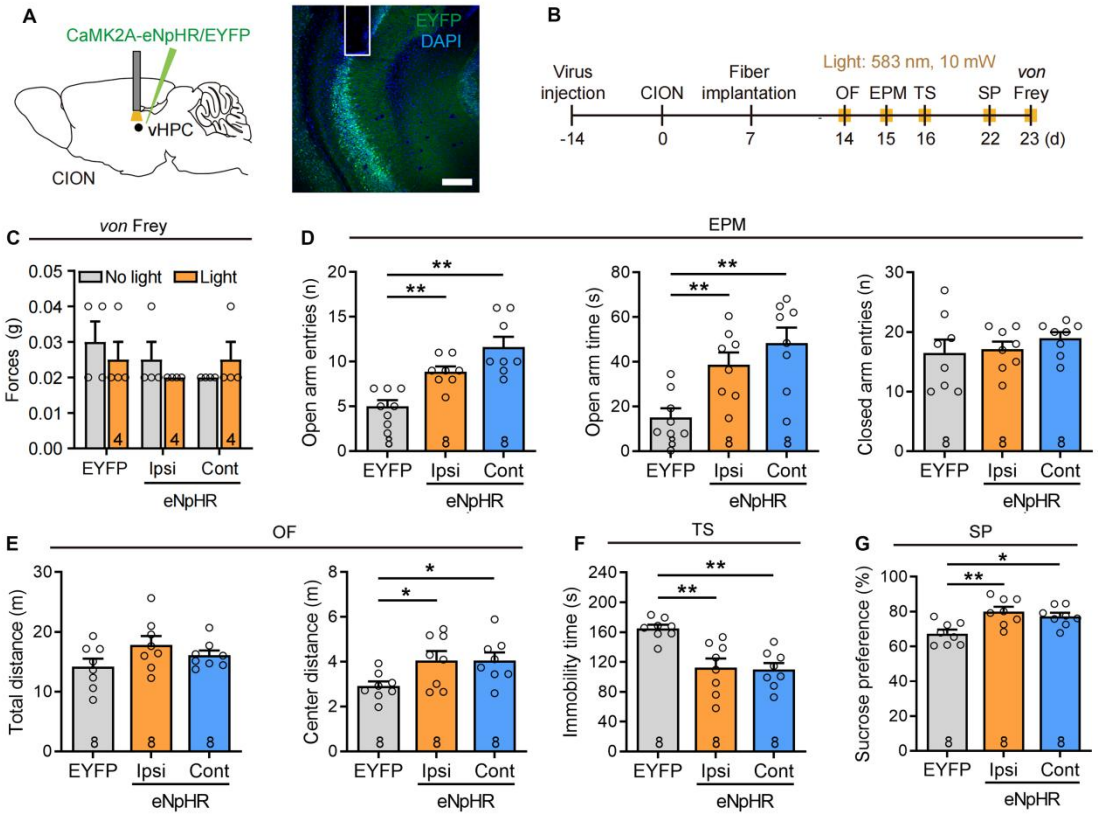

Fig. S4. Optogenetic inhibition of vHPC CaMK2A$^+$ excitatory pyramidal neurons improves CION-induced anxiodepressive-like behaviors. (A) Sagittal schematic and photomicrograph of coronal section showing specific infection of vHPC CaMK2A$^+$ neurons with eNpHR or EYFP. Scale bar: 200 μm. **(B)** Schematic of the protocol in experiments C-G. **(C)** Optogenetic inhibition of vHPC CaMK2A$^+$ neurons has no effect on CION-induced mechanical allodynia in the vibrissa pad. Two-way ANOVA. **(D-G)** Optogenetic inhibition of CaMK2A$^+$ neurons in both ipsilateral and contralateral vHPC effectively alleviates CION-induced anxiodepressive-like behaviors in EPM (D), OF (E), TS, (F), and SP (G) tests. *P<0.05, **P<0.01, two-tailed Student's t-test. Data are expressed as means ± SEM. Sample sizes are indicated in bars.

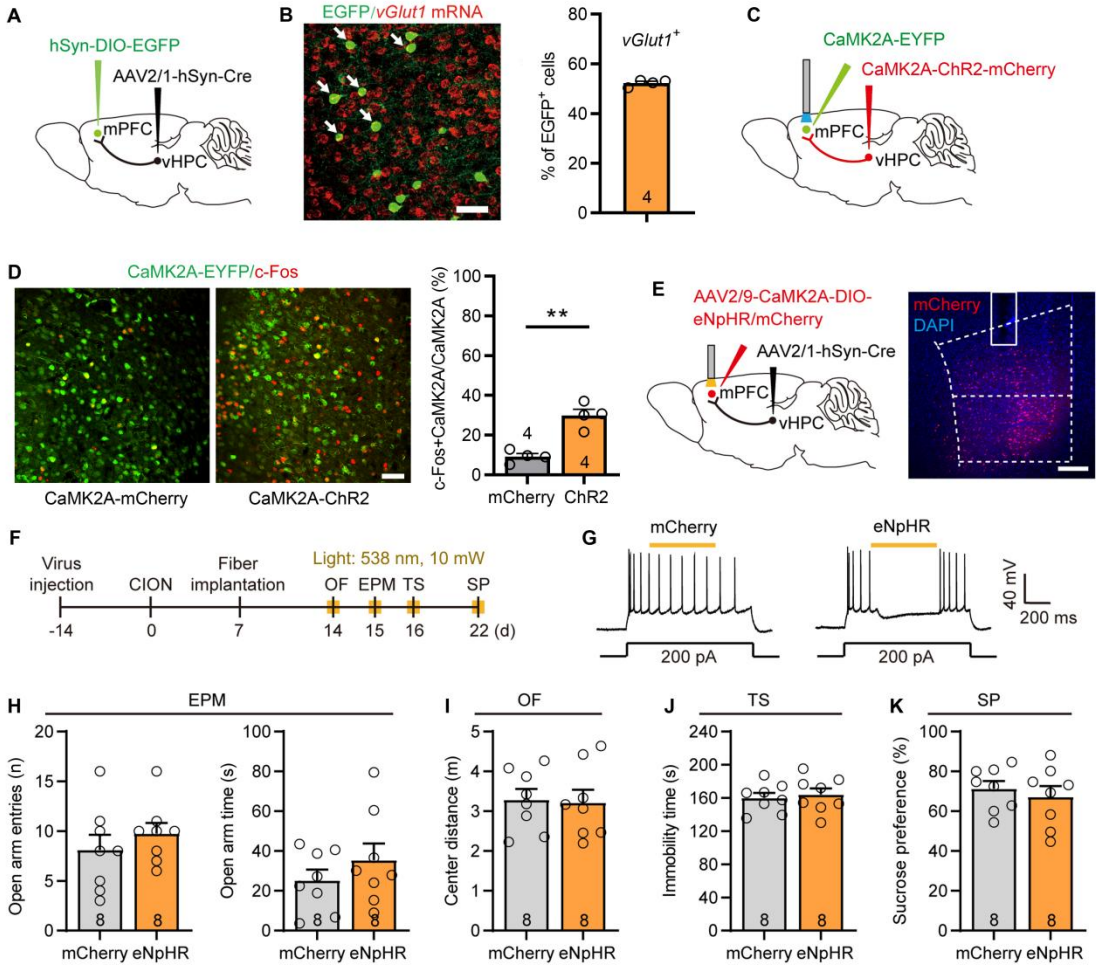

Fig. S5. Inhibition of vHPC-mPFC^{CaMK2A} projections does not affect CION-induced anxiodepressive behaviors. (A) Sagittal schematic showing specific infection of EGFP on mPFC postsynaptic neurons receiving projections from the vHPC. **(B)** RNAscope fluorescence *in situ* hybridization (FISH) showing colocalization and proportion of *vGlut1* mRNA with mPFC postsynaptic EGFP^{+} neurons receiving projections from the vHPC. Scale bar: 50 μm. (**C**) Sagittal schematic showing specific infection of EYFP on mPFC CaMK2A^{+} neurons, and optogenetic manipulation of vHPC^{CaMK2A}-positive terminals expressing ChR2 in the mPFC. **(D)** Optogenetic activation of

$vHPC^{CaMK2A}$-positive terminals expressing ChR2 in the mPFC upregulates c-Fos expression in $CaMK2A^+$ neurons in the mPFC. Scale bar: 100 μm. **P<0.01, two-tailed Student's t-test. **(E)** Sagittal schematic and photomicrograph of coronal section showing specific infection of eNpHR or mCherry on mPFC postsynaptic $CaMK2A^+$ neurons receiving projections from the vHPC. Scale bar: 200 μm. **(F)** Schematic of the protocol in experiments H–K. **(G)** Patch clamp recording in mPFC slices showing that APs are suppressed by yellow light stimulation in mPFC postsynaptic $CaMK2A^+$ neuron expressing eNpHR. **(H–K)** Optogenetic inhibiting mPFC postsynaptic $CaMK2A^+$ neurons receiving projections from the vHPC does not affect CION-induced anxiodepressive-like behaviors in EPM (H), OF (I), TS (J) and SP (K) tests. Two-tailed Student's *t*-test. Data are expressed as means ± SEM. Sample sizes are indicated in brackets and bars.

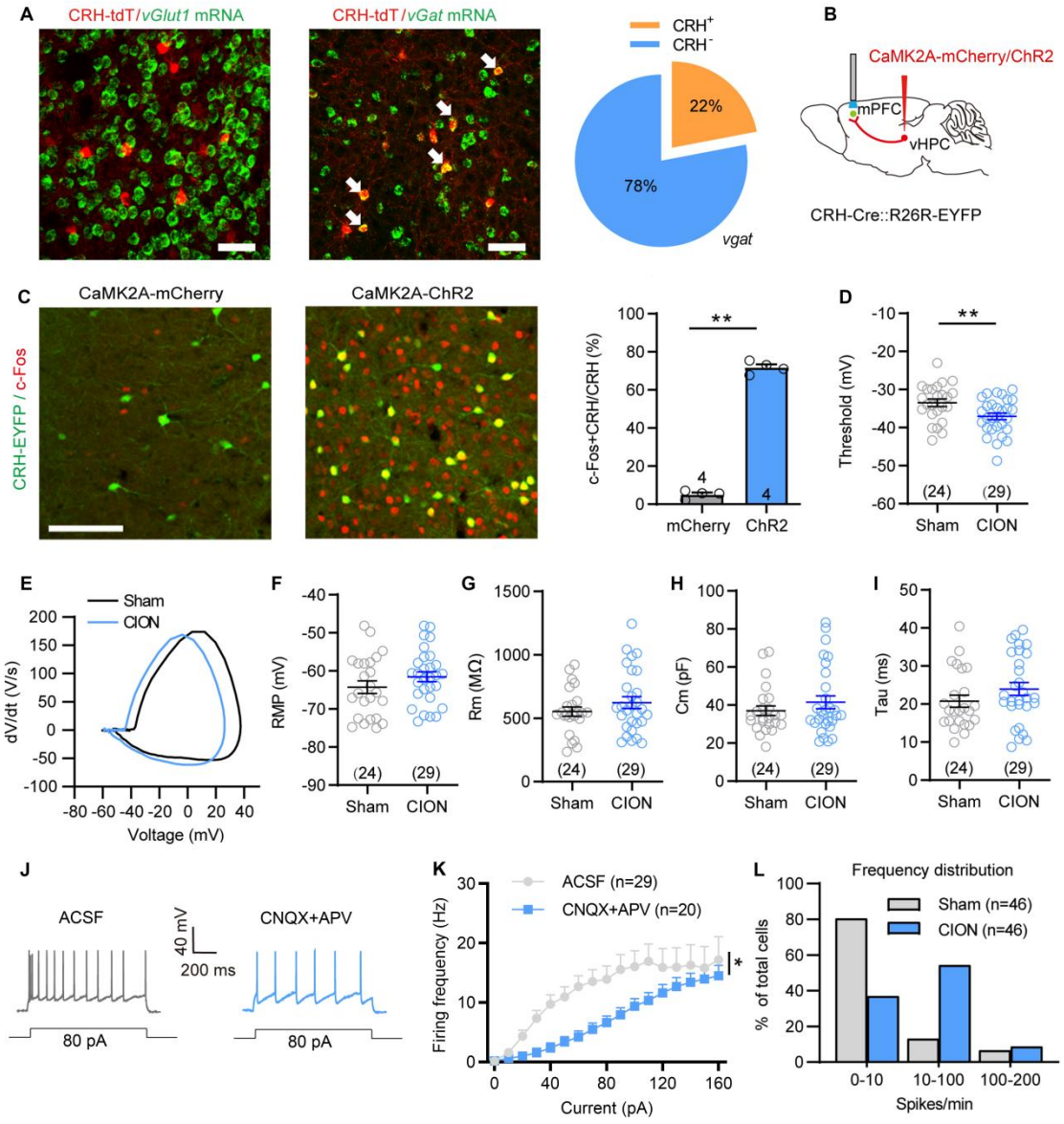

Fig. S6. The Distribution and electrophysiological properties of CRH^{+} neurons in the mPFC. (A) RNAscope FISH showing co-localization of *vGlut1* mRNA or *vGat* mRNA with CRH-tdTomato (CRH-tdT) neurons in the mPFC. Arrows indicates CRH-tdT and *vGat* mRNA double-labeled cells. Scale bar: 50 μm. **(B)** Sagittal schematic showing CaMK2A-ChR2 injection into the vHPC of CRH-Cre::R26R-EYFP and optogenetic manipulation of vHPC^{CaMK2A}-positive terminals expressing ChR2 in the mPFC. **(C)**

Optogenetic activation of $vHPC^{CaMK2A}$-positive terminals expressing ChR2 in the mPFC significantly upregulates c-Fos expression in CRH^+ neurons in the mPFC. Scale bar: 100 μm. **P<0.01, two-tailed Student's t-test. **(D)** CION mice have more hyperpolarized AP firing threshold in mPFC postsynaptic CRH^+ neurons. **P<0.01, two-tailed Student's t-test. **(E)** Phase plots of the APs evoked by brief current injections in mPFC postsynaptic CRH^+ neurons from sham, and CION-14d mice. **(F-I)** CION does not affect RMP (F), Rm (G), Cm (H) and Tau (I) of mPFC CRH^+ neurons on day 14 after sham and CION. Two-tailed Student's t-test. **(J, K)** Bath application of AMPA receptor antagonist CNQX (10 μM) and NMDA receptor antagonist APV (50 μM) partially blocks CION-induced excitatory effects on AP firing of mPFC postsynaptic CRH^+ neurons from CION-14d mice. *P<0.01, two-way RM ANOVA . Here, the gray line data (ACSF) are from Fig. 5I (CION) as a reference for CNQX+APV treatment group. **(L)** CION changes spontaneous APs frequency distribution in mPFC CRH^+ neurons by cell-attach recording. Data are expressed as means ± SEM. Sample sizes are indicated in bars and brackets.

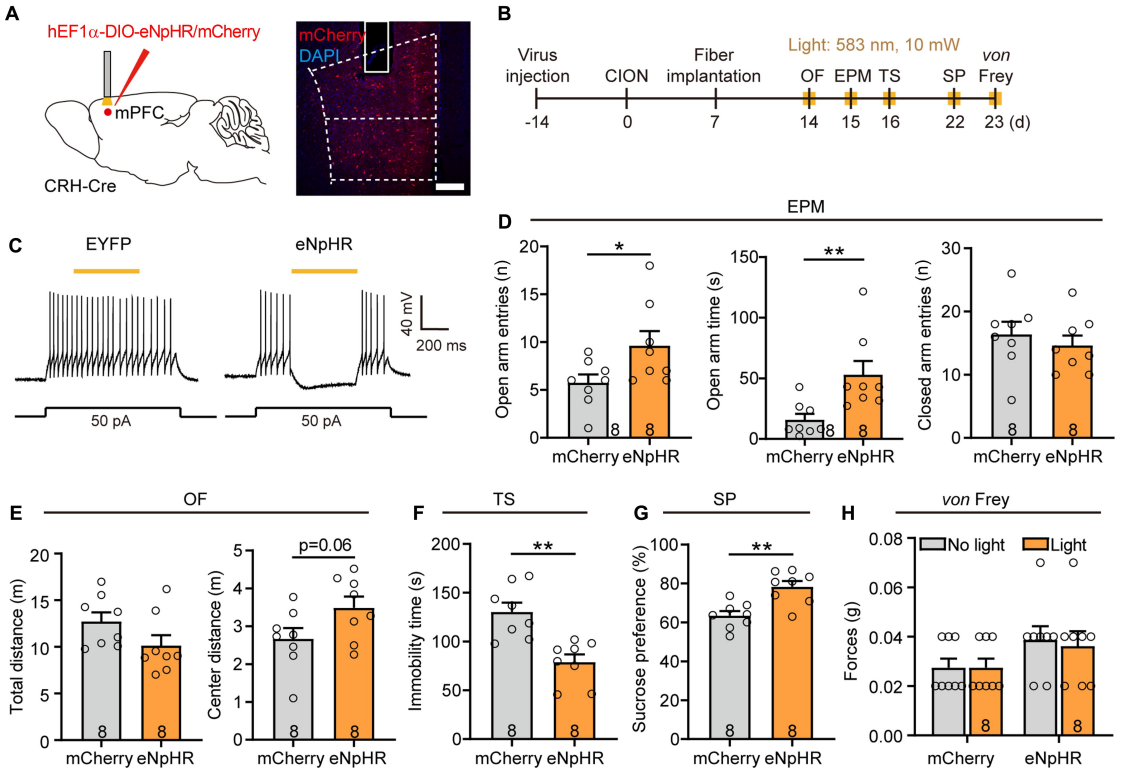

Fig. S7. Inhibition of mPFC CRH$^+$ neurons alleviates CION-induced anxiodepressive behaviors. (A) Sagittal schematic and photomicrograph of coronal section showing specific infection of eNpHR or EYFP on mPFC CRH$^+$ neurons in CRH-Cre mice. Scale bar: 200 μm. **(B)** Schematic of the protocol in experiments D-H. **(C)** Patch clamp recording in mPFC slice showing that APs are suppressed by yellow light stimulation (583 nm, 5 mW, continuous) in mPFC CRH$^+$ neurons expressing eNpHR. **(D-G)** Optogenetic inhibition of mPFC CRH$^+$ neurons produces antianxiodepressive-like behaviors in EPM (D), OF (E), TS (F), and SP (G) tests. **P<0.01, two-tailed Student's t-test. **(H)** Optogenetic inhibition of mPFC CRH$^+$ neurons does not affect CION-induced mechanical allodynia in the vibrissa pad in *von* Frey test. Two-tailed Student's t-test. Data are expressed as means ± SEM. Sample sizes are indicated in bars.

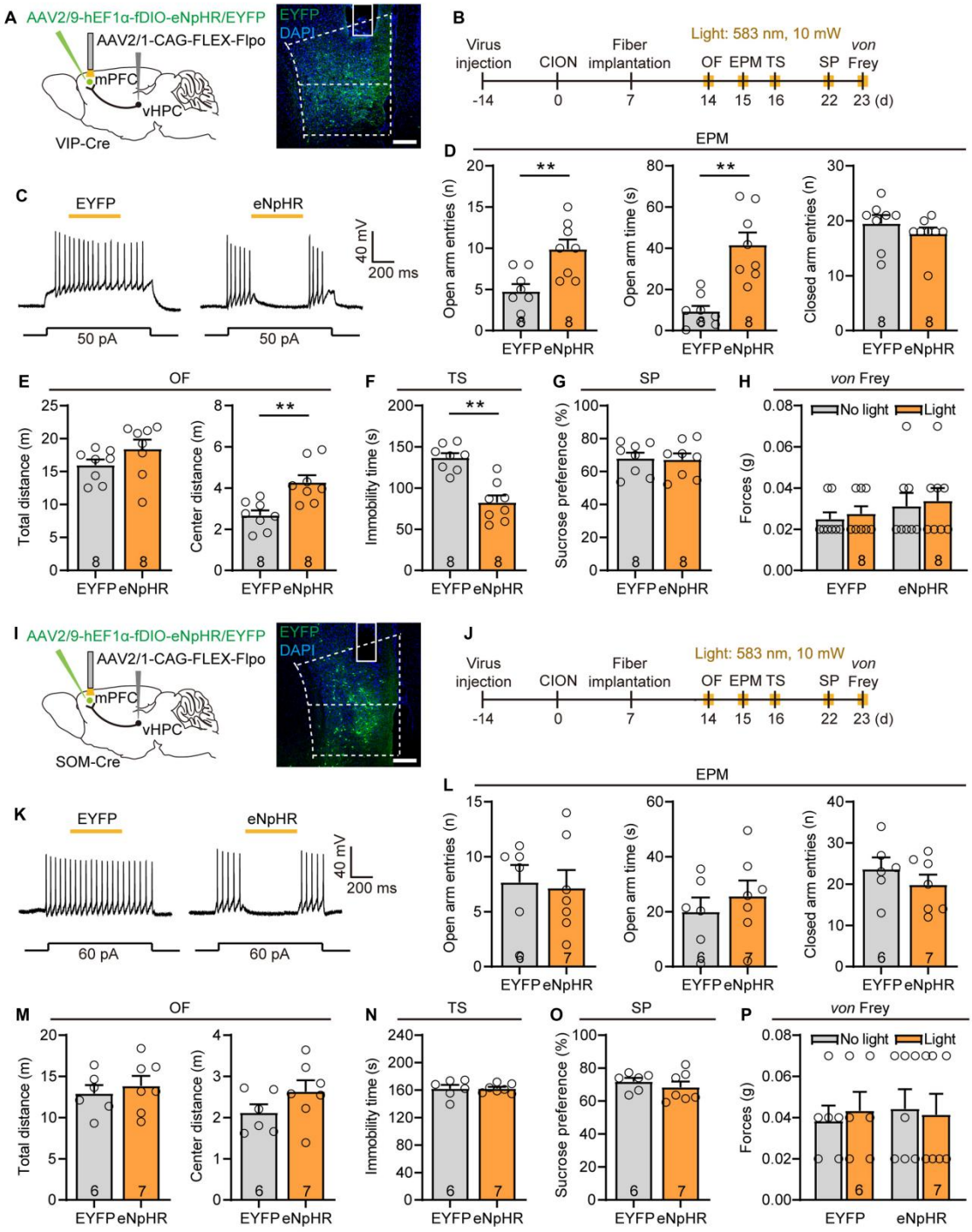

Fig. S8. Inhibition of vHPC-mPFC^{VIP} but not vHPC-mPFC^{SOM} pathway alleviates CION-induced anxiodepressive behaviors. (A) Sagittal schematic and photomicrograph of coronal section showing specific infection of eNpHR or EYFP on

mPFC postsynaptic VIP^+ neurons receiving projections from the vHPC in VIP-Cre mice. Scale bar: 200 μm. **(B)** Schematic of the protocol in experiments D-H. **(C)** Patch clamp recording in mPFC slice showing that APs are suppressed by yellow light stimulation (583 nm, 5 mW, continuous) in mPFC postsynaptic VIP^+ neurons expressing eNpHR. **(D-F)** Optogenetic inhibition of mPFC postsynaptic VIP^+ neurons receiving projections from the vHPC produces anti-anxiodepressive-like behaviors in EPM (D), OF (E), and TS (F), tests. **P<0.01, two-tailed Student's t-test. **(G, H)** Optogenetic inhibition of mPFC postsynaptic VIP^+ neurons does not affect CION-induced anhedonic-like phenotype in SP (G) test, and mechanical allodynia in the vibrissa pad in von Frey test (H). Two-tailed Student's t-test. **(I)** Sagittal schematic of photomicrograph of coronal section showing specific infection of eNpHR or EYFP on mPFC postsynaptic SOM^+ neurons receiving projections from the vHPC in SOM-Cre mice. Scale bar: 200 μm. **(J)** Schematic of the protocol in experiments L-P. **(K)** Representative traces showing that APs are suppressed by yellow light stimulation in mPFC postsynaptic SOM^+ neuron expressing eNpHR. **(L-P)** Optogenetic inhibition of mPFC postsynaptic SOM^+ neurons receiving projections from the vHPC does not affect CION-induced anxiodepressive-like behaviors and mechanical allodynia. Two-tailed Student's t-test for D-G, two-way ANOVA for H. Data are expressed as means ± SEM. Sample sizes are indicated in bars.

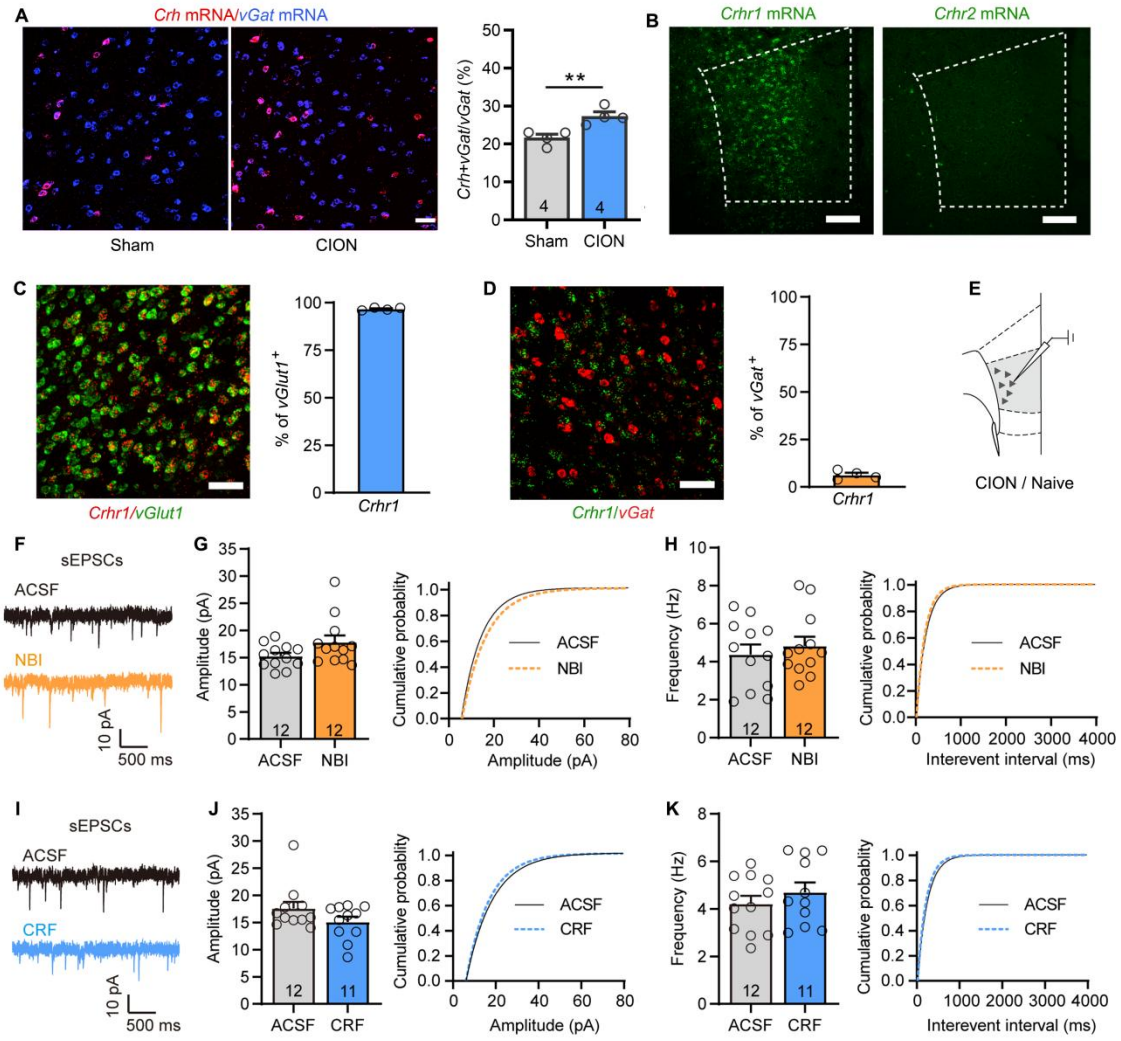

Fig. S9. Distribution of *Crh* and *Crh* receptors mRNA in the mPFC, and the effects of CRH-CRHR1 signaling on excitatory synaptic transmission in layer V mPFC pyramidal neurons. (A) RNAscope FISH showing upregulated *Crh* mRNA in *vGat*$^+$ mPFC neurons in CION-14d mice. **P<0.01, two-tailed Student's t-test. Scale bar: 50 μm. **(B)** RNAscope FISH showing distribution of *Crhr1* and *Crhr2* mRNA in the mPFC. Scale bar: 200 μm. **(C, D)** RNAscope FISH showing co-localization and proportion of *vGlut1* mRNA (C) or *vGat* mRNA (D) with neurons expressing *Crhr1* mRNA in layer V of the mPFC. Scale bar: 50 μm. **(E)** Schematic showing the location of the recorded

neurons in layer V mPFC pyramidal neurons in CION-14d and naive mice. **(F-H)** Patch clamp recording of sEPSCs showing that CRHR1 antagonist NBI27914 (5 μM) does not affect the amplitude and frequency of sEPSCs in CION-14d mice. Two-tailed Student's t-test. **(I-K)** Bath application of CRF (200 nM) does not affect the amplitude and frequency of sEPSCs in naive mice. Two-tailed Student's t-test. Data are expressed as means ± SEM. Sample sizes are indicated in bars.

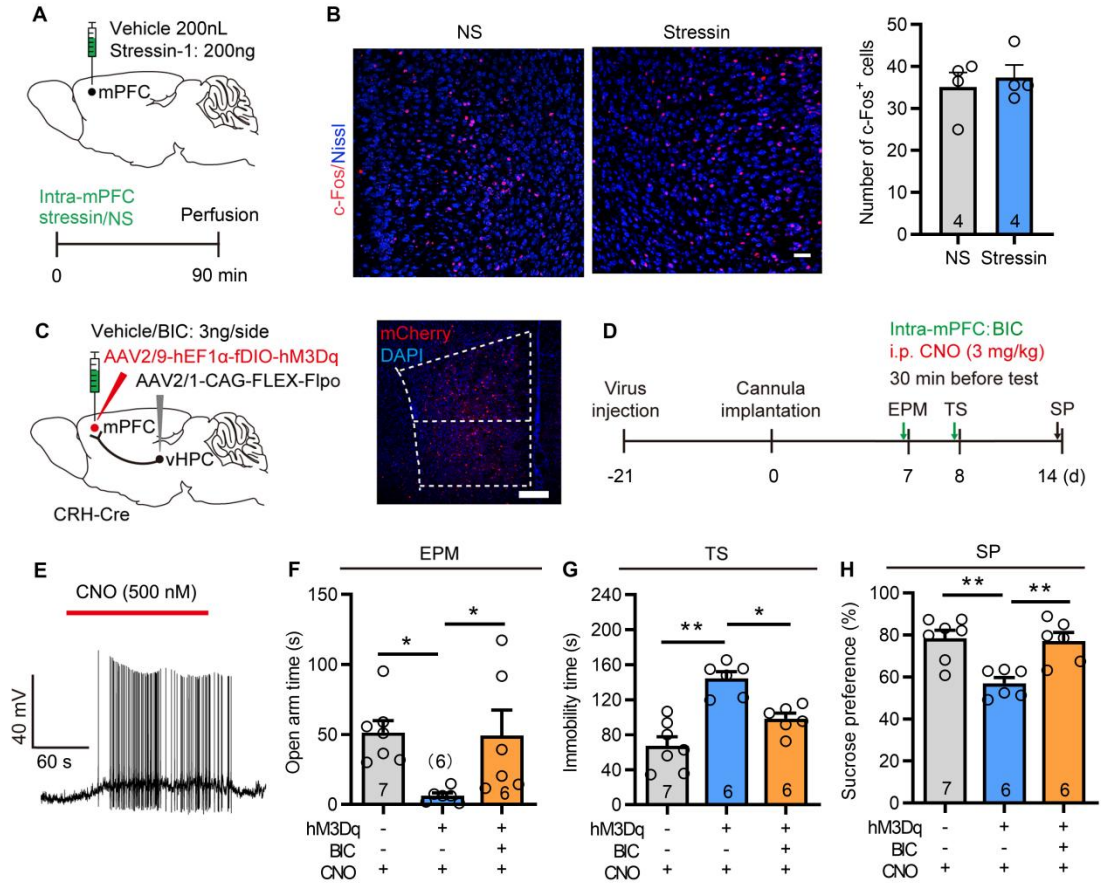

Fig. S10. GABA$_A$ receptors in the mPFC are involved in anxiodepressive-like behaviors mediated by the vHPC-mPFC^{CRH} pathway. (A) Sagittal schematic of intra-mPFC injection and the protocol for experiment B. **(B)** Compared with equal volume normal saline injection, intra-mPFC injection of CRHR1 agonist stressin-1 (200 ng/0.2 μL) does not alter c-Fos expression level in mPFC neurons. Scale bar: 50 μm. Two-tailed Student's *t*-test. **(C)** Sagittal schematic and photomicrograph of coronal section showing specific infection of hM3Dq or mCherry on mPFC postsynaptic CRH$^+$ neurons receiving projections from the vHPC and GABA$_A$ receptor antagonist BIC (3 ng/0.2μL) injection into the mPFC of CRH-Cre mice. Scale bar: 200 μm. **(D)** Schematic

of the protocol in experiments F-H. **(E)** In current clamp model, application of CNO (500 nM) evokes spontaneous APs in a mPFC postsynaptic CRH^+ neuron expressing hM3Dq. **(F-H)** Chemogenetic activation of mPFC postsynaptic CRH^+ neurons receiving projections from the vHPC produces anxiodepressive-like behaviors in naive mice, which is significantly improved by intra-mPFC injection of BIC in EPM (F), TS (G) and SP (H) tests. **P*<0.05, ***P*<0.01, one-way ANOVA followed by post hoc Dunn's test. Data are expressed as means ± SEM. Sample sizes are indicated in bars.

Table S1. The key resources and reagents used in the present study.

REAGENT or RESOURCE	SOURCE	IDENTIFIER
Antibodies		
Chicken polyclonal anti GFP (1:1000)	Aves labs	CAT# GFP-1020 RRID:AB_10000240
Rabbit anti-RFP (1:1000)	Rockland	CAT# 600-401-379s RRID:AB_11182807
Rabbit anti c-Fos (1:2000)	Abcam	CAT# ab190289 RRID: AB_2737414
Donkey anti-Rabbit 546 (1:500)	Invitrogen	CAT# A10040; RRID:AB_2534016
Donkey Anti-Chicken 488 (1:500)	Jackson	CAT# 703-545-155; RRID:AB_2340375
Donkey Anti-Rabbit 647 (1:500)	Jackson	CAT# 711-605-152; RRID: AB_2492288
Bacterial and Virus Strains		
AAV2/9-CaMKIIa-ChR2-EYFP (titer: 3.04×10^{12} V.G./ml)	BrainVTA, Wuhan	CAT# PT-0004
AAV2/9-CaMKIIa-ChR2-mCherry (titer: 1.06×10^{13} V.G./ml)	OBiO, Shanghai	CAT# 26975
AAV2/9-hEF1a-fDIO-ChR2 (titer: 1.44×10^{13} V.G./ml)	Taitool, Shanghai	CAT# S0404-9
AAV2/9-CaMKIIa-eNpHR-EYFP (titer: 8.14×10^{12} V.G./ml)	OBiO, Shanghai	CAT# 26971
AAV2/retro-CAG-tdTomato-WPRE-pA (titer: 1.23×10^{12}V.G./mL)	Sunbio, Shanghai	CAT# pmt114-retro
AAV2/9-EF1α-DIO-eNpHR-mCherry (titer: 2.48×10^{12} V.G./ml)	BrainVTA, Wuhan	CAT# PT-0007
AVV2/9-hEF1α-fDIO-eNpHR-EYFP (titer: 2.37×10^{13} V.G./ml)	Taitool, Shanghai	CAT# S0357-9
AAV2/9-CaMKIIa-DIO-eNpHR-mCherry (titer: 5.18×10^{12} V.G./ml)	BrainVTA, Wuhan	CAT# PT-2060
AAV2/9-hEF1α-fDIO-hM3Dq-mCherry (AAV2/9, titer: 1.32×10^{13} V.G./ml)	Taitool, Shanghai	CAT# S0337-9
AAV2/9-GAD67-DIO-hM4Di-mCherry (titer: 1.21×10^{13} V.G./ml)	OBiO, Shanghai	CAT# H15084

AAV2/9-CaMKIIa-GCaMP6s (titer: 2.72×10^{12} V.G./ml)	BrainVTA, Wuhan	CAT# PT-0110
AAV2/1-hSyn-Cre (titer: 1.05×10^{13} V.G./ml)	BrainVTA, Wuhan	CAT# PT-0136
AAV2/1-hSyn-Flpo (titer: 1.92×10^{13} V.G./ml)	Taitool, Shanghai	CAT# S0271-1
AAV2/1-CAG-FLEX-Flpo (titer: 1.52×10^{13} V.G./ml)	Taitool, Shanghai	CAT# S0273-1
AAV2/9-CaMKIIa-mCherry (titer: 4.68×10^{12} V.G./ml)	OBiO, Shanghai	CAT# AOV013
AAV2/9-CaMKIIa-EYFP (titer: 1.70×10^{13} V.G./ml)	OBiO, Shanghai	CAT# AOV016
AAV2/9-EF1α-DIO-mCherry (titer: 2.51×10^{12} V.G./ml)	BrainVTA, Wuhan	CAT# PT-0013
AAV2/9-hsyn-DIO-EGFP (titer: 1.51×10^{13} V.G./ml)	Sunbio, Shanghai	CAT# pmt465
AAV2/9-hEF1α-fDIO-mCherry (titer: 1.91×10^{13} V.G./ml)	Taitool, Shanghai	CAT# S0553-9
AVV2/9-hEF1α-fDIO-EYFP (titer: 1.53×10^{13} V.G./ml)	Taitool, Shanghai	CAT# S0253-9
AAV2/9-CaMKIIa-DIO-mCherry (titer: 2.60×10^{12} V.G./ml)	BrainVTA, Wuhan	CAT# PT-1167
AAV2/9-GAD67-DIO-mCherry (titer: 1.27×10^{13} V.G./ml)	OBiO, Shanghai	CAT# H19924
Chemicals, Peptides, and Recombinant Proteins		
CRF (human, rat) acetate salt	Bachem	CAT# 4011473 CAS 86784-80-7
Stressin I	Tocris	CAT# 1608 CAS TP2125
NBI 27914 hydrochloride	Tocris	CAT# 1591 CAS 1215766-76-9
1(S),9(R)-(-)-Bicuculline methbromide (BIC)	Sigma	CAT# B7561 CAS 66016-70-4
6-cyano-7-Nitroquinoxaline-2,3-dione (CNQX)	Sigma	CAT# C127 CAS 115066-14-3
2-Amino-5-phosphonovaleric acid (APV)	Sigma	CAT# A5282 CAS 76326-31-3
GDP-β-S	Sigma	CAT# G7637 CAS 97952-36-8

Clozapine-n-oxide (CNO)	MedChemExpress	CAT# HY-17366 CAS 34233-69-7
RNAscope probes		
RNAscope®Probe-Mm-Slc17a7-C3(vGlut1)	ACDBio	CAT# 416631-C3
RNAscope®Probe-Mm-Slc32a1-C2 (vGat)	ACDBio	CAT# 319191-C2
RNAscope® Probe- Mm-Crh-C1	ACDBio	CAT# 316091-C1
RNAscope® Probe- Mm-Crhr1-C1	ACDBio	CAT# 418011-C1
RNAscope® Probe- Mm-Crhr2-C1	ACDBio	CAT# 413201-C1
Experimental Models: Organisms/Strains		
CRH-ires-Cre	The Jackson Laboratory	JAX012704
VIP-ires-Cre	The Jackson Laboratory	JAX010908
SOM- ires-Cre	The Jackson Laboratory	JAX028864
Ai14	The Jackson Laboratory	JAX007914
R26R-EYFP	The Jackson Laboratory	JAX006148
Software and Algorithms		
GraphPad Prism 8	GrapPad Software	www.graphpad.com
pClamp 10.6	Molecular Devices	www.moleculardevices.com
MATLAB	MathWorks	ww2.mathworks.cn

Data file S1: Data statistics

Data file S2: Original data